Activation-dependent changes in receptor distribution and dendritic morphology in hippocampal neurons expressing $P2X_2$-green fluorescent protein receptors

Baljit S. Khakh*, W. Bryan Smith, Chi-Sung Chiu, Donghong Ju, Norman Davidson, and Henry A. Lester

Division of Biology, 156-29, California Institute of Technology, Pasadena, CA 91125

Contributed by Norman Davidson, February 21, 2001

ATP-gated $P2X_2$ receptors are widely expressed in neurons, but the cellular effects of receptor activation are unclear. We engineered functional green fluorescent protein (GFP)-tagged $P2X_2$ receptors and expressed them in embryonic hippocampal neurons, and report an approach to determining functional and total receptor pool sizes in living cells. ATP application to dendrites caused receptor redistribution and the formation of varicose hot spots of higher $P2X_2$-GFP receptor density. Redistribution in dendrites was accompanied by an activation-dependent enhancement of the ATP-evoked current. Substate-specific mutant T18A $P2X_2$-GFP receptors showed no redistribution or activation-dependent enhancement of the ATP-evoked current. Thus fluorescent $P2X_2$-GFP receptors function normally, can be quantified, and reveal the dynamics of $P2X_2$ receptor distribution on the seconds time scale.

ion channel | ATP | filopodia

Cationic P2X receptors mediate the "fast" milliseconds time scale actions of ATP in the nervous system (1, 2). The identity of most natively expressed P2X receptors is unclear, but many neurons express $P2X_2$ mRNA, $P2X_2$ proteins, and functional $P2X_2$-like receptors (2). For example, ATP mediates synaptic transmission in a portion of CA1 neurons (3), and postnatal hippocampal neurons express P2X receptors, which include $P2X_2$ subunits (3–7). Moreover, cytosolic ATP concentration is 1–5 mM, and ATP released during tissue damage activates neuronal P2X receptors in the periphery (1). ATP released as a synaptic transmitter and during ischemia of brain neurons may contribute to pathophysiology, but there are no available data on the cellular consequences of $P2X_2$ receptor activation or on the dynamic aspects of $P2X_2$ receptor distribution in brain neurons.

This study used $P2X_2$ receptors tagged with green fluorescent protein (GFP) in a quantitative method to study receptors expressed with recombinant Sindbis virus in embryonic hippocampal neurons. We report (*i*) the properties of functional GFP-tagged $P2X_2$ receptors, (*ii*) an optical and electrophysiological approach to measuring receptor numbers in living cells, and (*iii*) the cellular effects of P2X receptor activation.

Materials and Methods

Molecular Biology. By PCR the $P2X_2$ stop codon was removed and the FLAG (f) epitope was inserted in frame with the $P2X_2$ cDNA cDNA (9). In the same PCR we inserted an *Xho*I site in the DNA. We generated GFP37 (10) with a *Xho*I site before the start codon and subcloned it into $P2X_2$-f between the *Xho*I site 3′ of the FLAG epitope and *Hin*dIII in the pcDNA3 polylinker to yield $P2X_2$-GFP. The $P2X_2$-f-GFP fragment was inserted into pSinRep5 between the *Stu*I and *Apa*I sites, and infective Sindbis particles were generated with the use of the Sindbis Expression System (http://www.invitrogen.com/). Site-directed mutagenesis was performed on the cDNAs with the use of synthetic oligonucleotides to generate K69A and T18A mutants (Quick Change; Stratagene).

Electrophysiology and Imaging. All cell preparations, two-electrode voltage-clamp recording of oocytes, and whole-cell patch recording of hippocampal neurons were performed by previously described methods (5, 11). Puffs (5 ms) of ATP (100 μM) were applied directly by pressure microejection to dendrites, soma, or neurites of the cell under voltage clamp (5–20 psi; 1 psi = 6.89 kPa) from 7- to 10-MΩ pipettes, with the use of a Picospritzer II (General Valve, Fairfield, NJ). We imaged hippocampal neurons with an Olympus Fluoview confocal microscope and software (http://www.olympus.com), but all analysis was performed with NIH IMAGEJ (http://rsb.info.nih.gov/ij/) and with the Fluoview software. We used an Olympus $\times$40 oil-immersion objective with a numerical aperture of 1.3. We applied test solutions to cells during imaging by switching among an array of parallel quartz tubes (320 μm i.d. and 450 μm o.d., ending $\approx$0.2 mm from the cell).

Data Analysis. Data were analyzed with CLAMPFIT (Axon Instruments) or ORIGIN 5.0 (Microcal Software, Northampton MA; http://www.MICROCAL.com/). Data in the text and graphs are shown as mean $\pm$ SEM from n determinations as indicated. We estimated the size of the somatic compartment by applying -5 mV voltage jumps to neurons under voltage clamp (-60 mV) and with the use of the following relations: $R_s = \delta V / I_{in}$ and $C_m = \tau / R_s$, where R_s is the series resistance, δV is the change in voltage (5 mV), I_{in} is the amplitude of the instantaneous current, C_m is the capacitance, and τ is the time constant for the relaxation of the capacitive transient; we assumed a membrane capacitance of 0.92 pF/100 μm^2 (12). We measured the number of receptors in the somatic compartment by using the relation $I = n \cdot i \cdot p_o$, where I is the peak of the macroscopic current, i is the unitary current at -60 mV ($\approx$1 pA), p_o is the open probability (0.6), and n is the number of receptors open at the peak (13). For the optical determination of receptor density the measured pixel intensity was divided by 4 because the receptors are multimeric (1) and by 2 because $\approx$50% of the neuron surface is attached to the glass coverslip; the receptors here are not expected to be gated by ATP. The adjusted pixel intensity (14) was used to determine receptor numbers from standard curves (Fig. 2*F*). The coefficient of variance = SD divided by the mean for n trials, where the nth trial is at most 20.

Abbreviations: GFP, green fluorescent protein; wt, wild type.

*To whom reprint requests should be sent at present address: Medical Research Council, Laboratory of Molecular Biology, Cambridge CB2 2QH, United Kingdom. E-mail: bsk@mrc-lmb.com.ac.uk.

The publication costs of this article were defrayed in part by page charge payment. This article must therefore be hereby marked "*advertisement*" in accordance with 18 U.S.C. §1734 solely to indicate this fact.

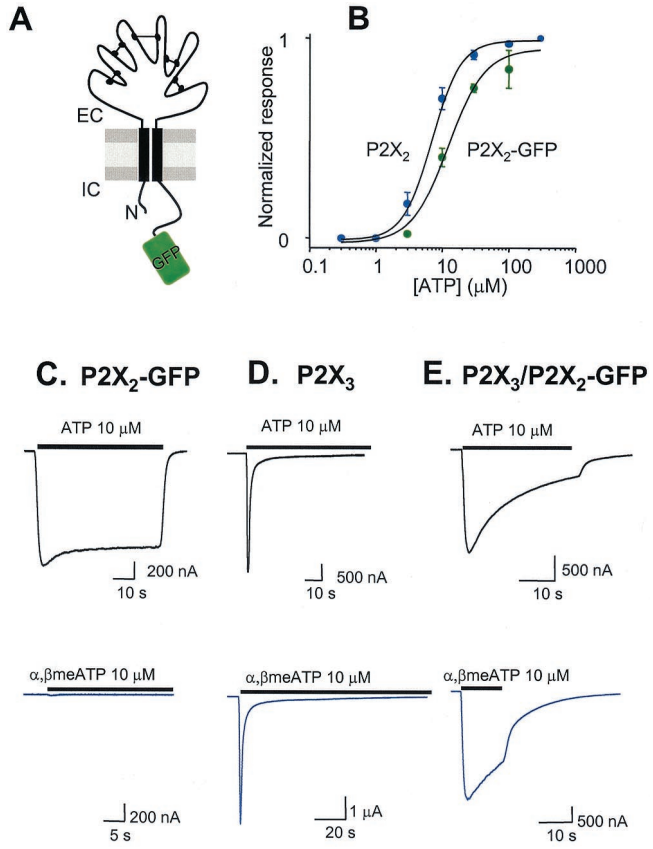

Fig. 1. Properties of $P2X_2$-GFP receptors. (*A*) Diagram of $P2X_2$-GFP receptor subunit topology. The folds in the extracellular loop represent hypothesized cysteine-cysteine linkages (1). (*B*) ATP concentration–effect curves for wt $P2X_2$ and $P2X_2$-GFP receptors. (*C–E*) Representative ATP and α,β-methylene-ATP-evoked current waveforms from cells expressing $P2X_2$-GFP (*C*), $P2X_3$ (*D*), and $P2X_3/P2X_2$-GFP receptors (*E*). The ATP-evoked currents desensitized by 16 ± 1%, 91 ± 1% ($\tau 1 = 0.9 \pm 0.2$ s, $\tau 2 = 9 \pm 2$ s), and 63 ± 3% for $P2X_2$, $P2X_3$, and $P2X_3/P2X_2$-GFP receptors, respectively. The α,β-methylene-ATP-evoked currents desensitized by 91 ± 5% ($\tau 1 = 1.0 \pm 0.1$ s, $\tau 2 = 13 \pm 2$ s) and 51 ± 6% for $P2X_3$ and $P2X_3/P2X_2$-GFP receptors, respectively.

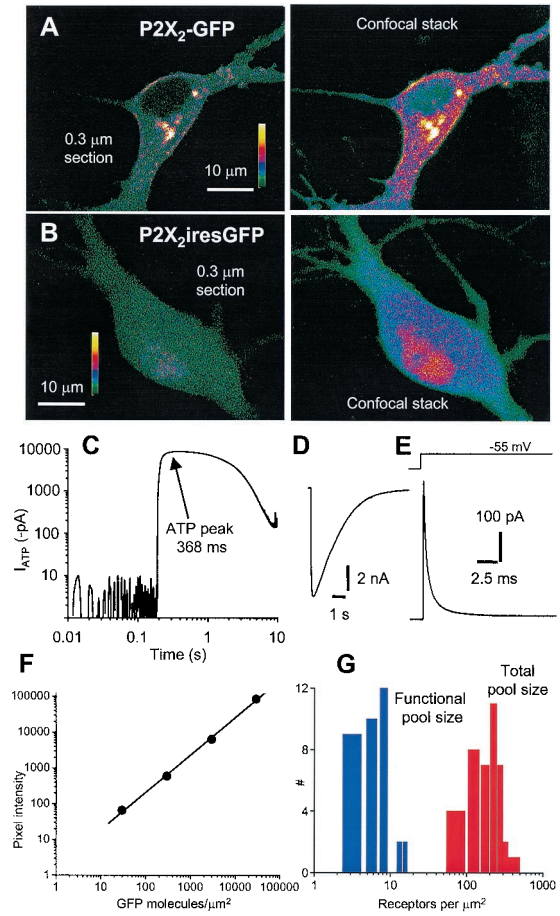

Fig. 2. Quantification of $P2X_2$-GFP receptors in embryonic hippocampal neurons. (*A*) (*Left*) An image through the soma of a neuron expressing $P2X_2$-GFP receptors. (*Right*) A confocal stack of 25 optical sections of the same neuron spaced at 0.3 μm. (*B*) (*Left*) An image through the soma of a neuron expressing GFP from a bicistronic $P2X_2$iresGFP mRNA. (*Right*) A confocal stack of 25 optical sections of the same neuron spaced at 0.3 μm. (*C*) Representative ATP-evoked current (100 μM, 0.5 s pulse on to soma) shown on double log scales to show that the peak was calculated at the plateau of the response at 368 ms (peak current −8.5 ± 0.5 nA, 10–90% rise time 82 ± 20 ms, 90–10% decay time 2.9 ± 0.2 s; $n = 36$). (*D*) The same current waveform as in *C*, but on linear scales. (*E*) Representative current in response to a 5 mV step from −60 mV. The trace was analyzed with the use of an equivalent circuit of the neuron somatic compartment, where V_p is the pipette potential (−60 mV), R_s is the series resistance (15 ± 1 MΩ), R_m is the membrane resistance (741 ± 119 MΩ), V_m is the membrane potential, and C_m is the membrane capacitance (24.5 ± 1.6 pF; all $n = 36$). (*F*) Standard curve of GFP fluorescence intensity for agarose beads with various densities of GFP bound to the surface (14). The pixel intensity is the fluorescence intensity per pixel^2 of the bead surface. For high GFP densities (>100,000 GFP molecules per μm^2) the intensity was saturating and thus measurements were made with a neutral density filter between the objective and the charge-coupled device, and the absolute values were corrected *post hoc* (14). (*G*) Distribution of numbers of $P2X_2$ receptors per μm^2.

Results

Properties of $P2X_2$ Receptors Tagged with GFP. We ligated GFP (10) in frame onto the C terminus of $P2X_2$ receptors (Fig. 1*A*). When expressed in *Xenopus* oocytes, $P2X_2$-GFP and wild-type (wt) receptors are similar with respect to ATP EC_{50} (Fig. 1*B*) peak currents, desensitization kinetics, and suramin block {ATP EC_{50} 6.5 ± 0.9 and 13.5 ± 1.5 μM, Hill slopes 1.7 ± 0.1 and 2.1 ± 0.2, for wt ($n = 8$) and $P2X_2$-GFP receptors ($n = 9$); 30 μM suramin block was 86 ± 11% and 91 ± 2%, and k_{+1} was 1.2 ± 0.4 and 1.2 ± 0.2 × 10^4 $M^{-1}\cdot s^{-1}$ for wt ($n = 3$) and $P2X_2$-GFP receptors ($n = 9$); where $k_{+1} = 1/\tau$[suramin]}. $P2X_2$-GFP receptors also formed a heteromer with $P2X_3$ (15), as indicated by a slowly desensitizing response to 10 μM α,β-methylene-ATP, whereas $P2X_2$-GFP receptors did not respond to this agonist and $P2X_3$ receptors responded with rapidly desensitizing currents (Fig. 1 *C–E*). Thus wt and $P2X_2$-GFP receptors are similar, with the exception that $P2X_2$-GFP receptors fluoresce under blue light and thus provide a noninvasive marker for receptor location in living cells (Fig. 2).

Density of $P2X_2$-GFP Receptors in Hippocampal Neurons. We used Sindbis virus constructs (16) to express $P2X_2$-GFP, GFP, $P2X_2$iresGFP, T18A $P2X_2$-GFP, or K69A $P2X_2$-GFP receptors in embryonic hippocampal neurons, which are devoid of P2X receptors at this stage of development (5). Confocal laser scanning microscopy revealed that expression of $P2X_2$-GFP resulted in green fluorescence that localized to the plasma membrane and the cytosol (Fig. 2*A*), whereas expression of $P2X_2$iresGFP resulted in cytosolic green fluorescence (Fig. 2*B*). Membrane and cytosolic $P2X_2$-GFP fluorescence was notable in 0.3 μm optical sections (Fig. 2*A*), demonstrating that some $P2X_2$-GFP receptors are cytosolic, as is the case for natively expressed P2X receptors (17, 18). Capacitance measurements showed that somatic membrane area was 2449 ± 159 μm^2 ($n = 36$), and by measuring the peak currents evoked by a pulse of 100

μM ATP (-8.5 ± 0.5 nA; $n = 36$, Fig. 2 *C* and *D*) we determined that the Sindbis vector directs the membrane expression of 6.3 ± 0.5 $P2X_2$-GFP receptors per μm^2 (Fig. 2 *G*; $n = 36$; see *Materials and Methods*), thus defining the somatic functional receptor pool size for these experiments.

We next exploited the fixed stoichiometry between $P2X_2$ and GFP in the fusion construct and used fluorescence microscopy to measure the somatic total $P2X_2$-GFP receptor pool size. The characterization used transparent beads with calibrated surface densities of GFP quantified with the use of an epifluorescence microscope (14) (Fig. 2*F*). We compared the fluorescence intensity of the soma with the fluorescence intensity per square micrometer of calibrated bead surface, which served as an optical standard (14). We found a value of 208 ± 14 receptors per μm^2 ($n = 42$) for the total somatic receptor pool size (Fig. 2*G*). Thus most $P2X_2$-GFP receptors are cytosolic, and this pool may be a source and sink for delivery to the plasma membrane.

ATP-Induced Formation of Varicose $P2X_2$-GFP Hot Spots. We collected images during a 1–5 min control period, then applied a pulse of either 100 μM glutamate or 100 μM ATP (10–30 s) and imaged filopodia with confocal laser scanning microscopy. We observed no change in the distribution of fluorescence with glutamate application, but during ATP application some areas increased in fluorescence; in addition, the apparent size of the fluorescent area increased within 5–10 s (Fig. 3 *A–D*). Thus ATP produced varicose hot spots (Fig. 3 *C* and *D*). The formation of varicosities was supported by similar observations in neurons infected with $P2X_2$iresGFP ($n = 8$), and this provides strong proof for a change in dendritic morphology. To quantify hot spot size we measured the intensity of pixels along a control line, during glutamate application and ATP application. Representative images of filopodia are shown in Fig. 3 *A–C*, and normalized plots for 23 line profiles are shown in Fig. 3*D*. Glutamate caused no change in the fluorescence profiles, but ATP increased the width of $P2X_2$-GFP receptor-expressing areas in regions where hot spots occur ($n = 23$). Hot spot width (at the base of the line profiles) was 1.8 ± 0.2 μm initially and 1.8 ± 0.2 μm with glutamate, but 2.9 ± 0.3 μm after ATP ($n = 23$). Thus the ATP-evoked hot spots in filopodia have a diameter approaching that of the varicosities, at ≈ 3 μm.

We next chose regions of interest, *post hoc,* where hot spots formed *de novo*. We compared data on regions of interest for 86 hot spots before and during ATP application. On average there was a net increase in pixel intensity or $P2X_2$-GFP receptors in regions of interest by $66 \pm 6\%$ ($n = 86$), but pixel intensity decreased in other nearby areas within the same filopodium (Fig. 3 *E* and *F*), and there was no net increase in spatially integrated intensity (Fig. 3*E*) over entire dendritic arbors. These data imply that $P2X_2$-GFP hot spots occur because existing receptors redistribute during activation (Fig. 3).

Simple ATP-evoked depolarization is not the cause of redistribution because glutamate (100 μM) and KCl (15 mM; data not shown) did not affect $P2X_2$-GFP distribution (Fig. 3). Furthermore, we observed no ATP-evoked currents or changes in the distribution of fluorescence in neurons that expressed GFP alone or mutant K69A $P2X_2$-GFP receptors (see *Materials and Methods*; $n = 4$, Fig. 4 *A* and *C*), in which ATP binding is disrupted (19). Therefore there are no native ATP receptors that contribute to either the optical or electrophysiological responses described in this study. This observation adds credence to the analysis used to determine receptor numbers (Fig. 2 and *Materials and Methods*)

P2X receptors have at least two open states (I_1 and I_2) that differ in their permeability to organic cations. The I_2 state is entered in an ATP-dependent manner, has higher permeability than the I_1 state to some cations (5, 11, 20–22), and is absent in mutant T18A P2X receptors (23) with a disrupted protein kinase C site in the amino tail (24). In contrast to $P2X_2$-GFP receptors, mutant T18A $P2X_2$-GFP receptors did not redistribute when ATP was applied ($n = 11$, Fig. 4 *B* and *C*). T18A $P2X_2$-GFP receptors displayed rapidly desensitizing ATP-evoked responses ($n = 16$; >95% desensitization, 90–10% decay time $= 0.9 \pm 0.1$ s, and 10–90% rise time $= 59 \pm 14$ ms for a 2.5 s 100 μM ATP pulse; Fig. 4*C*), whereas $P2X_2$-GFP responses desensitized by <10% ($n = 5$; Fig. 4*C*). T18A mutant receptors are useful because they allow $P2X_2$ receptor responses to be assigned to a particular channel state, and we interpret the rapid desensitization kinetics in T18A mutants as indicative of the presence of only the I_1 state (23). Overall these data imply that $P2X_2$-GFP receptor redistribution and varicosity formation require prolonged $P2X_2$ receptor function, for instance, as produced by the I_2 state.

Activation-Dependent Run-Up of the $P2X_2$ Current. Our imaging experiments show that $P2X_2$-GFP receptor activation causes redistribution of fluorescence and a change in morphology, but it remained unclear whether $P2X_2$-GFP receptors move in the plasma membrane as a result of activation. To address the latter, we tested electrophysiologically for stimulation-evoked changes in functional $P2X_2$ receptors by applying ATP briefly (4–10 ms) to soma and dendrites of hippocampal neurons to approach the brevity of synaptic ATP release (25).

When ATP was puffed at a frequency of less than 0.1 Hz, the measured responses differed only slightly from puff to puff by $\leq$10% (the coefficient of variance was $8.9 \pm 2.2\%$ within a train of 20 responses at 0.1 Hz, and the peak of the first puff was 560 ± 371 pA; $n = 3$). But, remarkably, at a frequency of 1 Hz, the ATP-evoked currents increased in amplitude by $254 \pm 45\%$ from 290 ± 64 pA at the first puff (Fig. 5*A*; $n = 12$ of 15 neurons; three neurons showed no run-up) of the initial amplitude within 10 responses. The increase could be described by a rate constant of ≈ 0.7 s^{-1} ($1/\tau$; Fig. 5*B*). The coefficient of variance for puffs 1 through 10 was $23.5 \pm 3.5\%$ ($n = 12$), reflecting the activation-dependent run-up of the ATP-evoked current, but for trials 11 through 20 the coefficient of variance was $5.5 \pm 2.2\%$ ($n = 12$). Our measurements indicate that $\approx$300 $P2X_2$ receptors are activated during the first puff and, on average, that the number of functional receptors doubles within 10 repetitive puffs at 1 Hz.

Run-up was not observed when glutamate was similarly applied to hippocampal neurons (35 ± 13 pA at first puff, $n = 3$; Fig. 5*B*), when ATP was applied to superior cervical ganglion neurons (87 ± 31 pA at first puff, $n = 5$; Fig. 5*B*), or when ATP was applied to hippocampal neurons expressing T18A $P2X_2$-GFP mutant receptors (1018 ± 121 pA at first puff; Fig. 5*B*). We also examined $P2X_3$ receptors in small-diameter dorsal root ganglion neurons; as expected, the ATP-evoked currents showed marked desensitization between trials (26) (426 ± 86 pA at first puff, $n = 15$; Fig. 5*B*). Accepting the limitation that the glutamate-evoked currents were smaller than the ATP-evoked currents, we interpret these data to indicate that the ATP response in hippocampal neurons (Fig. 5*A*) was not an artifact of the puffer.

Discussion

The present study shows that $P2X_2$ receptors tagged with GFP are functional. There were more $P2X_2$-GFP receptors in the cell than functional receptors in the membrane, and we present an electrophysiological and optical approach to measuring the number of functional receptors and the total number of receptors in living cells. We expect that similar approaches that use calibrated beads (14) as standards can be used to quantify the expression of any biologically interesting GFP-tagged proteins or organelles such as synaptic vesicles, in living cells in real time. In a previous study, $P2X_1$ receptors tagged with GFP on the C terminus were reported to internalize during ATP applications

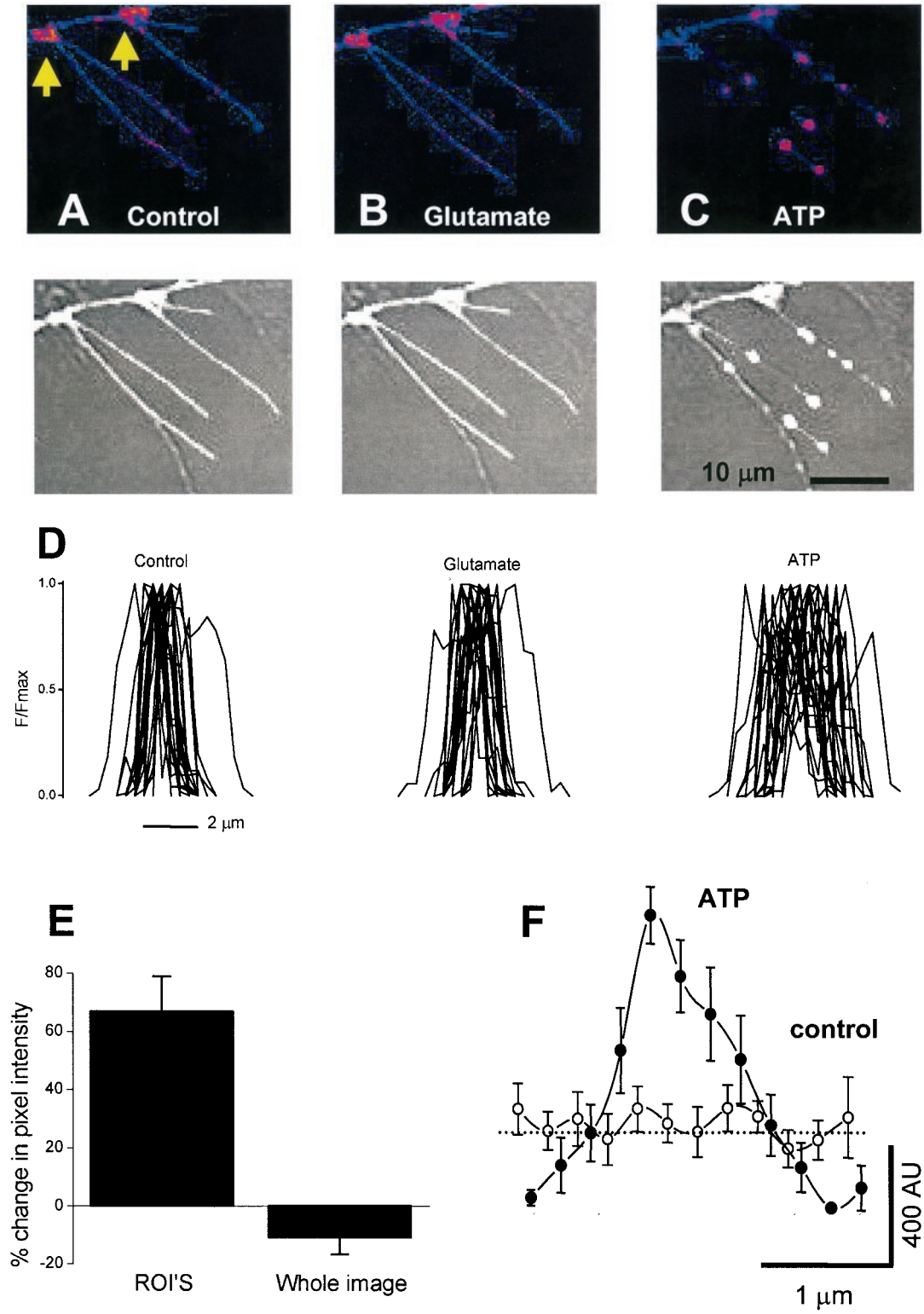

Fig. 3. ATP-dependent redistribution of P2X receptors in hippocampal neurons. (*A–C*) (*Upper*) False color images of filopodia from hippocampal neurons expressing $P2X_2$-GFP. (*Lower*) Overlay of gray-scale fluorescence and bright-field images. (*Left*) The control image. (*Center*) With 100 μM glutamate. (*Right*) With 100 μM ATP. (*D*) Twenty-three intensity profiles across filopodia for control, in glutamate, and in the presence of ATP. (*E*) ATP-evoked changes in integrated pixel intensity of whole dendritic arbors and regions of interest (ROI's). (*F*) Average line profile along 10 hot spots before and during ATP. AU, arbitrary units. Note the peak of the hot spot has higher fluorescence, but that $\approx$1 μm from the peak, the intensity falls to values lower than in the control.

(27). In contrast, we found no evidence for net internalization or externalization of $P2X_2$-GFP receptors expressed in hippocampal neurons when ATP was applied.

During $P2X_2$-GFP receptor activation by ATP, we observed (*i*) the formation of varicose hot spots, (*ii*) $P2X_2$-GFP redistribution over micrometer distances, and (*iii*) an activation-

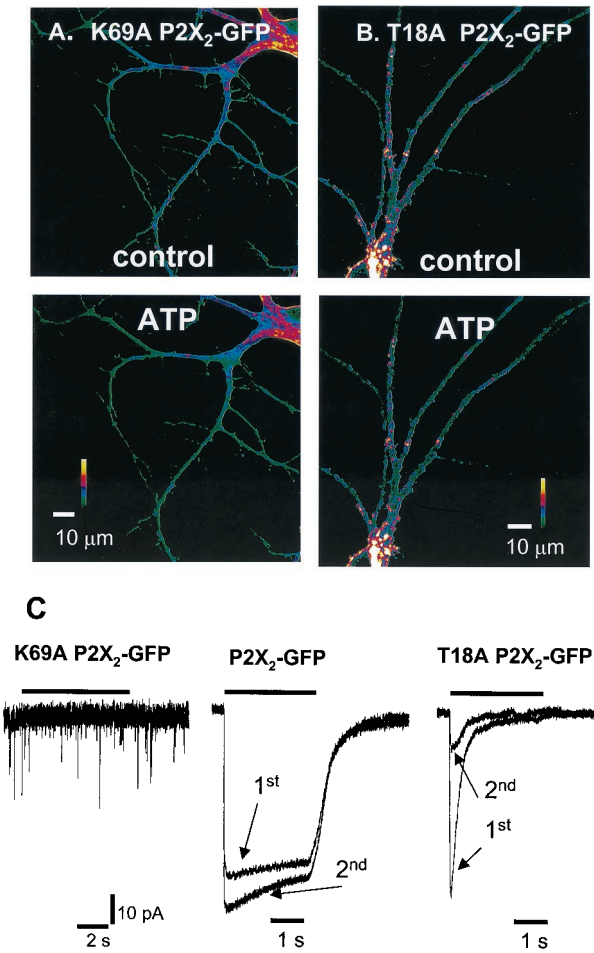

Fig. 4. $P2X_2$-GFP hot spots. (*A*) Representative examples of dendrites expressing K69A $P2X_2$-GFP receptors. ATP had no effect compared with the control. (*B*) Representative examples of dendrites expressing T18A $P2X_2$-GFP receptors. ATP had no effect compared with control. (*C*) (*Left*) 2.5s 100 μM ATP application did not evoke any membrane currents from this representative hippocampal neuron expressing K69A $P2X_2$-GFP receptors. The cells were healthy because glutamatergic excitatory postsynaptic currents were observed (downward deflections). (*Center*) 2.5 s 100 μM ATP-evoked currents (5 min apart) from a single hippocampal neuron expressing $P2X_2$-GFP receptors. The second response was larger than the first (see Fig. 5 for further experiments), and there was $<10\%$ desensitization. (*Right*) 2.5-s 100 μM ATP-evoked currents (5 min apart) from a single hippocampal neuron expressing T18A $P2X_2$-GFP receptors. Note that the second response is smaller than the first (see also Fig. 5). The traces in *Center* and *Right* are normalized to the peak of the first response.

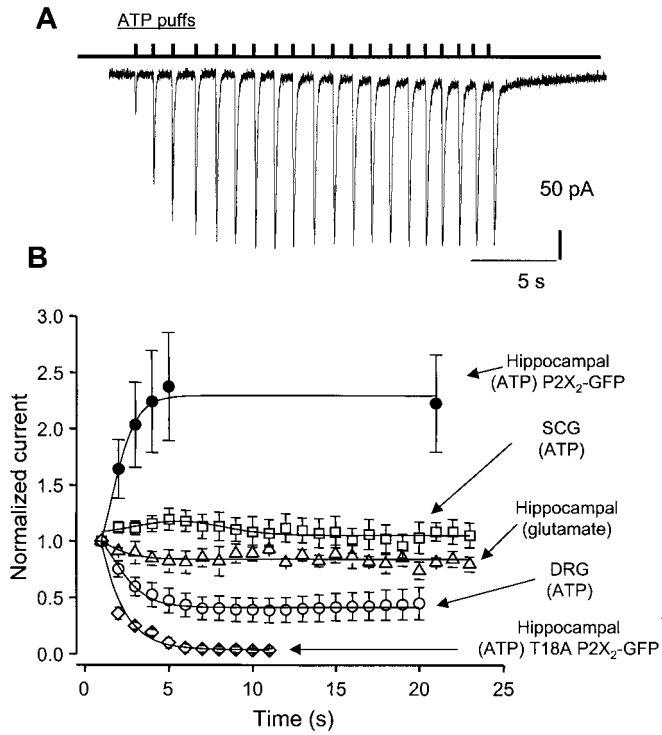

Fig. 5. Run-up of the P2X receptor current as a function of activation. (*A*) Representative whole-cell current recording with ATP puffed every second, for a total of 20 puffs. We could not reliably apply ATP at frequencies faster than 1 Hz. (*B*) Effect of repetitive applications of transmitter to neurons, with current normalized to the first puff. The ATP-evoked currents in hippocampal neurons increase as a function of puff number, but glutamate-evoked currents in hippocampal neurons and ATP-evoked currents in superior cervical ganglion (SCG) neurons do not. The ATP-evoked currents in dorsal root ganglion (DRG) neurons show a significant decrease in amplitude as a function of puff number, as do the ATP-evoked currents at T18A $P2X_2$-GFP receptors.

dependent enhancement of the ATP-evoked current. We detected a 66% increase in pixel intensity at the most obvious hot spots after exposure to ATP for 5–10 s. We also detected a 100% increase in ATP-evoked responses after five puffs at 1 Hz. We hypothesize that the clustering (Figs. 3*C* and 5*A*) evoked by the addition of ATP underlies the observed increase in responses to puffs of ATP. There was a difference between the electrophysiology and imaging experiments: whereas the activation-dependent current increase reversed in $\approx$10 s, the increase in pixel intensity and varicosity formation persisted for at least 5 min. Presumably, changes in dendritic morphology (varicosities) that are detected optically, but not electrophysiologically, may explain this difference. Indeed, bright-field images show a change in morphology, and a similar phenomenon was observed with $P2X_2$iresGFP, which directs the expression of cytosolic GFP.

Activation of glutamate receptors results in the formation of varicosities in neuronal processes (28), and the glutamate receptor subunit, GluR1, moves from a cytosolic pool to the plasma membrane during activity in hippocampal neurons (16). These *in vitro* studies are enlightening because glutamate-evoked morphological changes are implicated in the pathogenesis of ischemic neurotoxicity, and GluR1 redistribution may occur during synaptic plasticity (16). The present data are portentous because $P2X_2$ receptor-activation-dependent changes in neuron morphology and receptor distribution may also occur for natively expressed receptors *in vivo*. Indeed, $P2X_7$ receptor-mediated currents in microglial cells show activation-dependent increases (29), and activation of $P2X_7$ receptors evokes changes in cell morphology (30), although changes in $P2X_7$ receptor distribution were not reported. Moreover, changes in superior cervical ganglion neuron morphology occur during P2X receptor activation (11). Interestingly, $P2X_7$ receptors as well as P2X receptors in microglial cells and superior cervical ganglion neurons display the I_2 state. The mechanisms underlying P2X receptor-mediated changes in cell morphology are currently unknown, but our data suggest that the higher permeability I_2 state of $P2X_2$ receptors is required (5, 11, 20–22) and that perhaps changes previously associated with $P2X_7$ receptors (30) may also occur during activation of neuronal P2X receptors. Fluorescence redistribution and changes in ATP-evoked currents and morphology do not result in cell death because the effects were completely reversible with the brief (up to 10–30 s) applications tested in the present study. Moreover, because the T18A muta-

tion disrupts the protein kinase C consensus site of $P2X_2$ receptors (24), these data are consistent with, but do not prove, the idea that $P2X_2$ receptor properties and redistribution may be shaped by protein kinase C activity.

Native neuronal P2X receptors mediate ATP fast synaptic transmission in the peripheral, enteric, and central nervous systems and presynaptically modulate synaptic transmission (1). In the present paper we have studied $P2X_2$-GFP receptors in hippocampal neurons because these cells are known to express $P2X_2$ receptors (17) and ATP mediates a component of the excitatory postsynaptic current (3). In view of the activation-dependent nature of the redistribution, $P2X_2$ receptor-mediated excitatory postsynaptic currents may undergo short-term modulation, by a postsynaptic mechanism similar to that suggested for glutamatergic synapses (8, 16, 31, 32). Moreover, P2X receptor-mediated changes in neuron morphology may be relevant during stroke when ATP is released. Our data establish redistribution and the formation of varicosities as an interesting functional attribute of heterologously expressed neuronal $P2X_2$-GFP receptors. It remains to be determined whether these effects occur for natively expressed receptors *in vivo*, either physiologically or during disease.

We thank H. Li for preparation of *Xenopus* oocytes and E. Schuman for advice and use of the confocal microscope. This work was supported by a Wellcome Trust (U.K.) Prize Fellowship (to B.S.K.), by a Roche Bioscience Award, and by the National Institutes of Health (NS-11756, MH 49176).

1. Khakh, B. S. (2001) *Nat. Rev. Neurosci.* **2,** 165–174.
2. Khakh, B. S., Burnstock, G., Kennedy, C., King, B. F., North, R. A., Seguela, P., Voigt, M. & Humphrey, P. P. A. (2001) *Pharmacol. Rev.*, **53,** 107–118.
3. Pankratov, Y., Castro, E., Miras-Portugal, M. T. & Krishtal, O. (1998) *Eur. J. Neurosci.* **10,** 3898–3902.
4. Wong, A. Y., Burnstock, G. & Gibb, A. J. (2000) *J. Physiol. (London)* **527,** 529–547.
5. Khakh, B. S., Proctor, W. R., Dunwiddie, T. V., Labarca, C. & Lester, H. A. (1999) *J. Neurosci* **19,** 7289–7299.
6. Collo, G., North, R. A., Kawashima, E., Merlo-Pich, E., Neidhart, S., Surprenant, A. & Buell, G. (1996) *J. Neurosci.* **16,** 2495–2507.
7. Kidd, E. J., Grahames, C. B., Simon, J., Michel, A. D., Barnard, E. A. & Humphrey, P. P. (1995) *Mol. Pharmacol.* **48,** 569–573.
8. Carroll, R. C., Lissin, D. V., von Zastrow, M., Nicoll, R. A. & Malenka, R. C. (1999) *Nat. Neurosci.* **2,** 454–460.
9. Brake, A. J., Wagenbach, M. J. & Julius, D. (1994) *Nature (London)* **371,** 519–523.
10. Grabner, M., Dirksen, R. T. & Beam, K. G. (1998) *Proc. Natl. Acad. Sci. USA* **95,** 1903–1908.
11. Khakh, B., Bao, X., Labarca, C. & Lester, H. (1999) *Nat. Neurosci.* **2,** 322–330.
12. Gentet, L. J., Stuart, G. J. & Clements, J. D. (2000) *Biophys. J.* **79,** 314–320.
13. Ding, S. & Sachs, F. (1999) *J. Gen. Physiol.* **113,** 695–720.
14. Chiu, C.-S., Kartalov, E., Unger, M., Quake, S. & Lester, H. A. (2001) *J. Neurosci. Methods*, **105,** 55–63.
15. Lewis, C., Neidhart, S., Holy, C., North, R. A., Buell, G. & Surprenant, A. (1995) *Nature (London)* **377,** 432–435.
16. Shi, S. H., Hayashi, Y., Petralia, R. S., Zaman, S. H., Wenthold, R. J., Svoboda, K. & Malinow, R. (1999) *Science* **284,** 1811–1816.
17. Rubio, M. E. & Soto, F. (2001) *J. Neurosci.* **21,** 641–653.
18. Gu, B. J., Zhang, W. Y., Bendall, L. J., Chessell, I. P., Buell, G. N. & Wiley, J. S. (2000) *Am. J. Physiol.* **279,** C1189–C1197.
19. Jiang, L.-H., Rassendren, F., Surprenant, A. & North, R. A. (2000) *J. Biol. Chem.* **275,** 34190–34196.
20. Virginio, C., MacKenzie, A., Rassendren, F. A., North, R. A. & Surprenant, A. (1999) *Nat. Neurosci.* **2,** 315–321.
21. Khakh, B. S. & Lester, H. A. (1999) *Neuron* **23,** 653–658.
22. Surprenant, A., Schneider, D. A., Wilson, H. L., Galligan, J. J. & North, R. A. (2000) *J. Auton. Nerv. Syst.* **81,** 249–263.
23. Khakh, B. S., Zhou, X., Sydes, J., Galligan, J. J. & Lester, H. A. (2000) *Nature (London)* **406,** 405–410.
24. Boue-Grabot, E., Archambault, V. & Seguela, P. (2000) *J. Biol. Chem.* **275,** 10190–10195.
25. Zhou, X. & Galligan, J. J. (1996) *J. Physiol. (London)* **496,** 719–729.
26. Cook, S. P., Rodland, K. D. & McCleskey, E. W. (1998) *J. Neurosci.* **18,** 9238–9244.
27. Li, G. H., Lee, E. M., Blair, D., Holding, C., Poronnik, P., Cook, D. I., Barden, J. A. & Bennett, M. R. (2000) *J. Biol. Chem.* **275,** 29107–29112.
28. Emery, D. G. & Lucas, J. H. (1995) *Brain Res.* **292,** 161–173.
29. Chessell, I. P., Michel, A. D. & Humphrey, P. P. (1997) *Br. J. Pharmacol.* **121,** 1429–1437.
30. Virginio, C., MacKenzie, A., North, R. A. & Surprenant, A. (1999) *J. Physiol. (London)* **519,** 335–346.
31. Lissin, D. V., Carroll, R. C., Nicoll, R. A., Malenka, R. C. & von Zastrow, M. (1999) *J. Neurosci.* **19,** 1263–1272.
32. Carroll, R. C., Beattie, E. C., Xia, H., Luscher, C., Altschuler, Y., Nicoll, R. A., Malenka, R. C. & von Zastrow, M. (1999) *Proc. Natl. Acad. Sci. USA* **96,** 14112–14117.